4D flow MRI in ascending aortic aneurysms: reproducibility of hemodynamic parameters

Juffermans, J.F.; Assen, H.C. van; Kiefte, B.J.C. te; Ramaekers, M.J.F.G.; Palen, R.L.F. van der; Boogaard, P. van den; ... ; Westenberg, J.J.M.

applied sciences

MDPI

Article

4D Flow MRI in Ascending Aortic Aneurysms: Reproducibility of Hemodynamic Parameters

Joe F. Juffermans [1,*], Hans C. van Assen [1], Bastiaan J. C. te Kiefte [1], Mitch J. F. G. Ramaekers [1,2,3,4], Roel L. F. van der Palen [5], Pieter van den Boogaard [1], Bouke P. Adriaans [2,3,4], Joachim E. Wildberger [3,4], Ilona A. Dekkers [1], Arthur J. H. A. Scholte [6], Simon Schalla [2,3,4], Hildo J. Lamb [1] and Jos J. M. Westenberg [1]

1 Department of Radiology, Leiden University Medical Center, 2333 ZA Leiden, The Netherlands; h.c.van_assen@lumc.nl (H.C.v.A.); b.j.c.te_kiefte@lumc.nl (B.J.C.t.K.); mitch.ramaekers@mumc.nl (M.J.F.G.R.); p.j.van_den_boogaard@lumc.nl (P.v.d.B.); i.a.dekkers@lumc.nl (I.A.D.); h.j.lamb@lumc.nl (H.J.L.); j.j.m.westenberg@lumc.nl (J.J.M.W.)
2 Department of Cardiology, Maastricht University Medical Center, 6229 HX Maastricht, The Netherlands; bouke.adriaans@mumc.nl (B.P.A.); s.schalla@mumc.nl (S.S.)
3 Department of Radiology and Nuclear Medicine, Maastricht University Medical Center, 6229 HX Maastricht, The Netherlands; j.wildberger@mumc.nl
4 Cardiovascular Research Institute Maastricht, 6229 HX Maastricht, The Netherlands
5 Division of Pediatric Cardiology, Department of Pediatrics, Leiden University Medical Center, 2333 ZA Leiden, The Netherlands; r.vanderpalen@lumc.nl
6 Department of Cardiology, Leiden University Medical Center, 2333 ZA Leiden, The Netherlands; a.j.h.a.scholte@lumc.nl
* Correspondence: j.f.juffermans@lumc.nl

check for updates

Citation: Juffermans, J.F.; van Assen, H.C.; te Kiefte, B.J.C.; Ramaekers, M.J.F.G.; van der Palen, R.L.F.; van den Boogaard, P.; Adriaans, B.P.; Wildberger, J.E.; Dekkers, I.A.; Scholte, A.J.H.A.; et al. 4D Flow MRI in Ascending Aortic Aneurysms: Reproducibility of Hemodynamic Parameters. *Appl. Sci.* **2022**, *12*, 3912. https://doi.org/10.3390/app12083912

Academic Editor: Qi-Huang Zheng

Received: 18 March 2022
Accepted: 11 April 2022
Published: 13 April 2022

Publisher's Note: MDPI stays neutral with regard to jurisdictional claims in published maps and institutional affiliations.

Abstract: (1) Background: Aorta hemodynamics have been associated with aortic remodeling, but the reproducibility of its assessment has been evaluated marginally in patients with thoracic aortic aneurysm (TAA). The current study evaluated intra- and interobserver reproducibility of 4D flow MRI-derived hemodynamic parameters (normalized flow displacement, flow jet angle, wall shear stress (WSS) magnitude, axial WSS, circumferential WSS, WSS angle, vorticity, helicity, and local normalized helicity (LNH)) in TAA patients; (2) Methods: The thoracic aorta of 20 patients was semi-automatically segmented on 4D flow MRI data in 5 systolic phases by 3 different observers. Each time-dependent segmentation was manually improved and partitioned into six anatomical segments. The hemodynamic parameters were quantified per phase and segment. The coefficient of variation (COV) and intraclass correlation coefficient (ICC) were calculated; (3) Results: A total of 2400 lumen segments were analyzed. The mean aneurysm diameter was 50.8 ± 2.7 mm. The intra- and interobserver analysis demonstrated a good reproducibility (COV = 16–30% and ICC = 0.84–0.94) for normalized flow displacement and jet angle, a very good-to-excellent reproducibility (COV = 3–26% and ICC = 0.87–1.00) for all WSS components, helicity and LNH, and an excellent reproducibility (COV = 3–10% and ICC = 0.96–1.00) for vorticity; (4) Conclusion: 4D flow MRI-derived hemodynamic parameters are reproducible within the thoracic aorta in TAA patients.

Keywords: aorta; aneurysm; hemodynamic; 4D flow MRI; reproducibility

1. Introduction

Patients with a thoracic aortic aneurysm (TAA) have an increased risk for aortic rupture and dissection [1]. Clinical guidelines use a maximal cross-sectional diameter ≥55 mm as the main criterion for the recommendation of preemptive surgical aortic replacement [2,3]. However, the majority (60–96%) of dissections occur in aortas with diameters below this threshold [4,5]. Therefore, there is a need for additional and more sensitive markers to identify patients at high risk of progressive dilation or adverse aortic events [6].

Evaluation of aortic hemodynamics is considered to be highly promising for the prediction of progressive dilatation and adverse aortic events [7–14]; the blood flow over the

cardiac cycle through the aorta can be analyzed using three-dimensional time-resolved phase-contrast magnetic resonance imaging (MRI), also known as four-dimensional (4D) flow MRI. From 4D flow MRI data, several relevant patient-specific hemodynamic parameters can be assessed. It has been demonstrated for patients with a tricuspid aortic valve (TAV) that the amount of flow displacement (a measure of eccentricity in the flow profile) is associated with aortic growth [7,8]. Furthermore, TAV patients showed decreased levels of vortical flow, helical flow, and wall shear stress (WSS) compared to healthy volunteers [9,10].

While such hemodynamic parameters could also be important for future clinical risk stratification of aneurysm patients, the majority of the studies assessing their agreements between observers and examinations only included healthy volunteers, patients with bicuspid aortic valves, or patients with mildly dilated aortas [13–22]. Hence, the reported outcomes are not fully translatable to TAA patients with substantially dilated aortas and a TAV. Therefore, the reproducibility of the hemodynamic parameters in such patients remains unknown [1]. Moreover, several previous studies quantified parameters based on (multiple) two-dimensional plane quantifications or ranked them qualitatively [15–18,21]. Thus, part of the spatial information is lost. In addition, the reproducibility of the WSS magnitude (WSS_{mag}) has been assessed well, but little is known about the reproducibility of the axial or circumferential WSS component (WSS_{ax}, WSS_{cir}, respectively) and the angle between both WSS components (WSS_{angle}).

To allow quantification of hemodynamic parameters in 4D flow MRI data, a cardiac phase-specific 3D lumen segmentation is required [23,24]. The shape of these lumen segmentations can be described by morphologic parameters such as the volume, centerline length, maximal diameter, and curvature radius. Interestingly, a recent study demonstrated that the curvature radius of the ascending aorta is associated with aortic growth [7].

In most commercial and research software tools, these lumen segmentations are constructed (semi-)automatically on the 4D flow MRI data and then manually adjusted when needed. The manual interaction may introduce observer-dependent variability in the quantitation of the hemodynamic parameters [25,26]. This observer-dependent variability of the 3D lumen segmentation can be assessed directly by evaluating the variability in morphologic parameters. The reproducibility of these morphologic parameters from 4D flow MRI data has been primarily reported in healthy volunteers [25].

Consequently, the aim of this study was to evaluate intra- and interobserver reproducibility of hemodynamic parameters, i.e., normalized flow displacement, flow jet angle, wall shear stress (magnitude, axial, circumferential, and angle), vorticity and helicity (absolute and local normalized) quantitatively assessed for six thoracic aortic lumen segments in patients with TAA and normally functioning TAV. In addition, intra- and interobserver reproducibility of morphological parameters, i.e., aortic volume, centerline length, lumen diameter, and curvature radius, were assessed.

2. Materials and Methods

2.1. Study Population

The study protocol was conducted in accordance with the Declaration of Helsinki and was approved by the local Medical Ethics Committee of the Leiden University Medical Center (G20.149, 9 October 2020), which waived the patient's informed consent for anonymized clinical data. The clinical database was used to identify TAA patients with a TAV who underwent a 4D flow MRI of the thoracic aorta between October 2018 and August 2021 (n = 260). Patients with aortic valve stenosis, regurgitation, or previous aortic surgery were excluded to obtain a selection of TAA patients without other pathologies, which potentially could also affect the reproducibility (n = 171). The clinical reports of the patients were evaluated for the maximal aortic diameter, and the 20 patients with the largest reported maximal diameters were included, see Figure 1. The presence of an aortic root or ascending aorta aneurysm was classified according to Della Corte's classification [27].

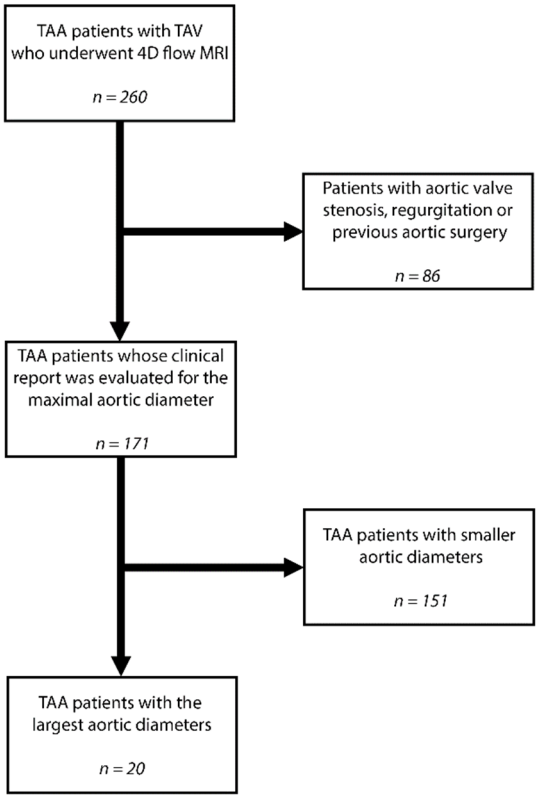

Figure 1. Population selection diagram. Abbreviations: TAA—thoracic aortic aneurysm, TAV—tricuspid aortic valve, MRI—magnetic resonance imaging, and 4D—four dimensional.

2.2. MRI Acquisition

The MRI examinations consisted of a 4D flow scan covering the entire thoracic aorta (for details, see Supplementary Materials Table S1). All subjects were scanned with a 3T-scanner (Ingenia or Elition, Philips Healthcare, Best, The Netherlands) using a FlexCoverage anterior and dStream Torso posterior coil. Concomitant gradient correction was performed using standard available scanner software. All data were visually inspected, and the absence of aliasing in the 4D flow MRI data was confirmed.

2.3. Image Analysis

The image analysis consisted of three parts: 4D flow MRI lumen segmentation, aorta morphology quantification, and hemodynamic quantification. First, the aortic lumen of the patients was segmented twice by the first observer (J.J.) and once by the second and third observers (M.R. and B.K., respectively). Lumen segmentation was performed using CAAS MR Solutions v5.2.1 (Pie Medical Imaging, Maastricht, The Netherlands). The software generated initial segmentations on the peak systolic phase and two consecutive phases before and after this peak systolic phase (i.e., five systolic phases, see Figure 2 and Supplementary Materials Video S1). Next, the aortic segmentations were manually corrected for all five phases and partitioned into six consecutive segments by manually placing anatomical planes perpendicular to the aortic centerline, respectively: the aortic root (from the aortic valve to the sinotubular junction), proximal ascending aorta (from the sinotubular junction to the mid-ascending aorta, defined as the midpoint on the centerline between the sinotubular junction and brachiocephalic artery), distal ascending aorta (from the mid-ascending aorta to the brachiocephalic artery), aortic arch (from the brachiocephalic artery until past the left subclavian artery), the proximal descending aorta (from the left subclavian artery to the mid-descending thoracic aorta, defined as the midpoint on the centerline between the left subclavian artery and the descending aorta at the level of the aortic valve), and distal descending aorta (from the mid-descending thoracic aorta to the

descending aorta at the level of the aortic valve). More details about the aortic segmentation are described by van der Palen et al. [20]. In addition, the stroke volume and cardiac output were assessed at the level of the sinotubular junction by the first observer for characterizing the left ventricular function of the population using CAAS MR Solutions.

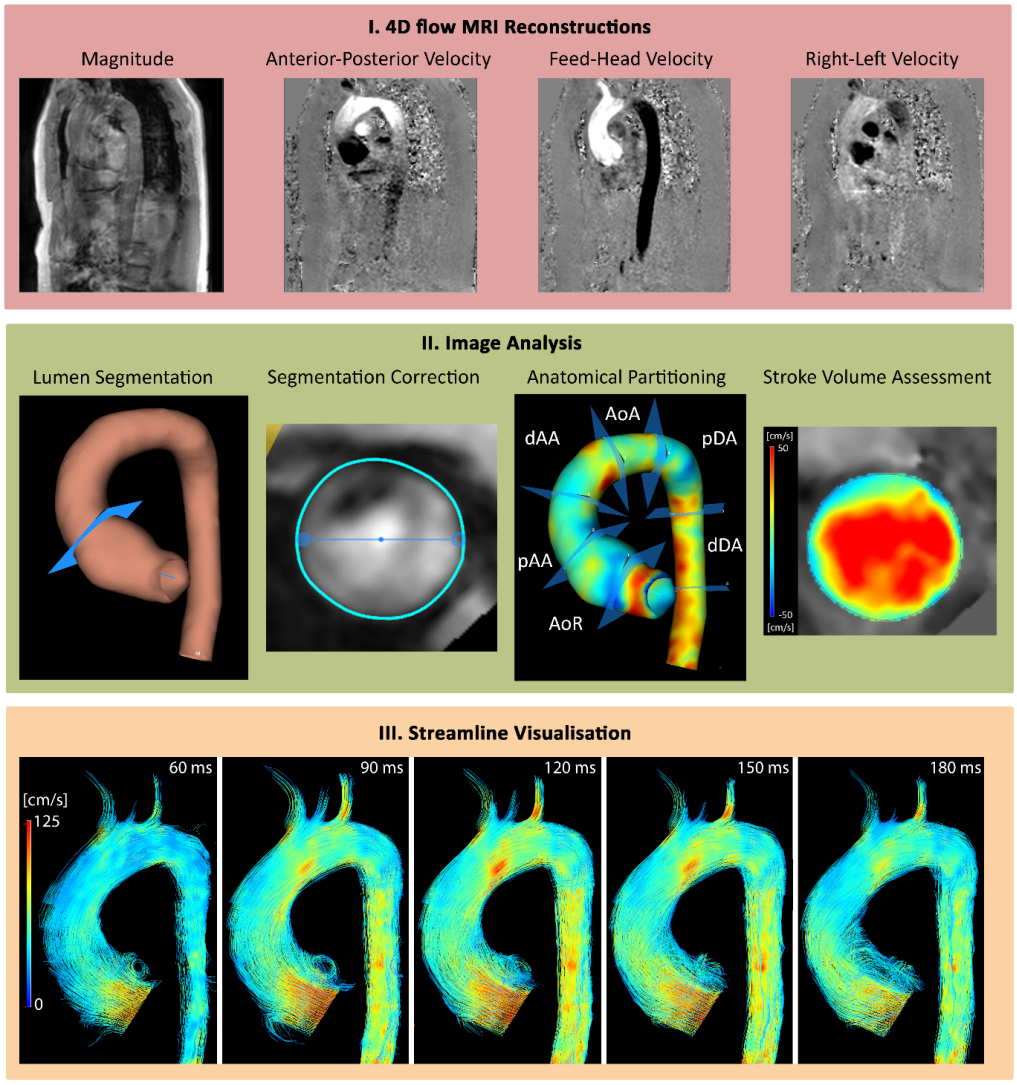

Figure 2. 4D flow MRI visualization using CAAS MR Solutions v.5.2.1. Example of a patient (male, 45 years old) with aortic root aneurysm with a diameter of 52 mm. (**I**) 4D flow MRI reconstructions. (**II**) Image analysis including the lumen segmentation, the manual segmentation correction, anatomical partitioning visualized on the wall shear stress maps, and stroke volume assessment. (**III**) Streamline visualization of the 4D flow MRI at the 5 systolic phases (60, 90, 120, 150, and 180 ms). Abbrevations: AoR—aortic root, pAA—proximal ascending aorta, dAA—distal ascending aorta, AoA—aortic arch, pDA—proximal descending aorta, and dDA—distal descending aorta. Secondly, the morphology of the thoracic aortas was analyzed using an in-house developed Python software (Python Software Foundation, Wilmington, DE, USA). This tool was used to quantify aortic volume, centerline length, maximal diameter, and curvature radius of each anatomical segment and for each of the five systolic phases. The aortic diameter was determined by first constructing a cross-section perpendicular to the centerline at every millimeter. Next, at each cross-section, the maximal radial spike length was calculated. The curvature radius was derived by fitting a circle through the segments' centerline as previously described [25]. The maximal aortic diameter within each segment and the radius of the fitted circle were used for statistical analysis.

Thirdly, the hemodynamics of the thoracic aorta were quantified using methods described in previous studies [13,15,19]. These methods were implemented in an in-house developed Python software [9,25]. Initially, the mean blood velocity over all subjects was quantified per anatomical segment. The tool was then used to quantify the normalized flow displacement, flow jet angle, vorticity norm, absolute helicity, and absolute LNH for each anatomical segment and each systolic phase. The normalized flow displacement and jet angle were determined by first constructing a cross-section perpendicular to the centerline at every millimeter. Next, at each cross-section, the normalized flow displacement (distance between the centerline point and center of velocity normalized for the vessel diameter times 100%) and flow jet angle (angle between the centerline and mean velocity vector) were calculated as previously described [15]. The maximal normalized flow displacement and flow jet angle within each segment were assessed and used for statistical analysis. For the calculation of vorticity and helicity of the velocity vector fields ($\underset{V}{\rightarrow}$), a spatial Gaussian differential operator ($\underset{\nabla}{\rightarrow}$) with a standard deviation equal to the reconstructed in-plane voxel size was used. The vorticity ($\underset{\omega}{\rightarrow} = \underset{\nabla}{\rightarrow} \times \underset{V}{\rightarrow}$) norm and absolute helicity ($H = |\underset{V}{\rightarrow} \cdot \underset{\omega}{\rightarrow}|$) were quantified via methods previously described by Ramaekers et al. [9]. The vorticity norm and absolute helicity were both normalized for the reconstructed voxel size, and the mean values within each segment were used for statistical analysis. Since a previous study demonstrated that a threshold of >0.6 for absolute LNH ($LNH = \frac{\underset{V}{\rightarrow} \cdot \underset{\omega}{\rightarrow}}{|\underset{V}{\rightarrow}||\underset{\omega}{\rightarrow}|}$) is the optimal criterion for detecting differences between patients and healthy volunteers [13], this threshold was used in our study to select volumes with increased absolute LNH. The volumes with increased absolute LNH were assessed and used for the statistical analysis. The in-house developed software can be made available for scientific collaboration per reasonable request. To derive 3D WSS maps for each of the five systolic phases, CAAS MR Solutions v5.2 was used. At each point of the 3D WSS map, WSS_{mag} was calculated as well as the WSS_{ax} and WSS_{cir} components. The WSS_{angle} between the WSS_{cir} and WSS_{ax} was quantified for each point as previously described [19]. For each anatomical segment, the mean WSS_{mag}, WSS_{ax}, $WSS_{cir,}$ and WSS_{angle} were used for statistical analysis.

2.4. Observer Training

All observers were acquainted with CAAS MR Solutions software. The first, second, and third observer had 4, 3, and 1 years' experience with lumen segmentation on 4D flow MRI data in TAA patients, respectively. Since the observers were recruited at two clinical centers and observers had different levels of experience, all observers received feedback on the segmented aorta from an experienced cardiovascular MRI researcher (J.J.M.W. with >15 years of 4D flow MRI experience) after analyzing the training cohort (n = 10 TAA patients). Hereafter, the results of the training cohort were not improved. Next, the observers analyzed the validation cohort (n = 10 TAA patients).

2.5. Statistical Analysis

Statistical analysis was performed using the open-source SciPy v1.2.1. software [28]. Parametric and non-parametric data are expressed as mean ± standard deviation (SD) or median (Q1–Q3), respectively. The Shapiro–Wilk test was used to verify the normality of the data. To assess the intra- and interobserver reproducibility, Bland–Altman analysis was performed, and the coefficient of variation (COV), Spearman rank correlation coefficient (r), and intraclass correlation coefficient (ICC) (two-way mixed effects, absolute agreement) were calculated. For the Bland–Altman analysis, the mean difference and limits of agreement (LoA = 1.96 × SD) were computed [29]. In addition, the relative difference in LoA between the training and validation cohort was calculated (LoA_{diff} = ((validation LoA–training LoA)/training LoA) × 100%). The COV was classified as low (≤10%), intermediate (11–20%), high (21–30%), or very high (>30%). The r and ICC were classified

as poor (<0.50), moderate (0.50–0.69), good (0.70–0.84), very good (0.85–0.94), or excellent (≥0.95) [25]. A p-value of <0.05 was considered statistically significant.

3. Results

The patient characteristics are presented in Table 1. In Table 2, median values of hemodynamic and morphologic parameters are presented. Of the selected TAA patients, 13 presented with an aneurysm in the aortic root and 7 with an ascending aorta aneurysm. The mean TAA diameter and mean blood velocity were 50.8 ± 2.7 mm and 42.5 ± 14.9 cm/s, respectively.

Table 1. Population characteristics.

Characteristic	Quantity
Population size	20
Male (%)	18 (90%)
Age (years)	53 ± 14
Height (cm)	186 ± 8
Weight (kg)	90 ± 11
TAA diameter (mm)	50.8 ± 2.7
Heart rate (bpm)	68 ± 11
Stroke Volume (mL)	105 ± 24
Cardiac Output (L min^{-1})	7.0 ± 1.8
Systolic blood pressure (mm Hg)	132 ± 14
Diastolic blood pressure (mm Hg)	81 ± 7
Trigger delay peak systole—2 phases (ms)	102 ± 31
Trigger delay peak systole—1 phase (ms)	133 ± 32
Trigger delay peak systole (ms)	163 ± 34
Trigger delay peak systole + 1 phase (ms)	194 ± 35
Trigger delay peak systole + 2 phases (ms)	224 ± 36

Data notated as the mean ± standard deviation and presented over all subjects. Abbreviation: TAA—thoracic aortic aneurysm.

Table 2. The hemodynamic and morphologic characteristics assessed in the thoracic aorta.

Parameter	Anatomical Segments					
	AoR	pAA	dAA	AoA	pDA	dDA
Flow Displacement (%)	7.5 (5.3–10.2)	9.8 (7.1–16.2)	6.3 (4.9–9.0)	5.7 (4.7–6.5)	6.5 (5.8–7.6)	4.7 (4.1–5.7)
Flow Jet Angle (°)	17.6 (13.7–21.9)	17.6 (11.9–27.0)	14.8 (10.2–21.3)	14.6 (12.5–17.3)	15.7 (13.1–18.4)	9.1 (7.6–10.6)
WSS magnitude (mPa)	561 (483–654)	763 (570–896)	750 (595–955)	746 (560–992)	877 (706–1112)	939 (785–1179)
Axial WSS (mPa)	371.9 (335–478)	627.9 (432–734)	702.6 (551–893)	700.6 (525–949)	801.5 (670–1045)	915.2 (748–1145)
Circumferential WSS (mPa)	331 (286–410)	331 (247–405)	204 (159–262)	182 (153–215)	243 (180–296)	205 (147–244)
WSS angle (°)	42.5 (37.4–45.7)	32.0 (26.8–37.1)	18.3 (13.7–24.0)	14.0 (12.1–16.9)	16.8 (14.4–20.2)	11.7 (9.6–14.4)
Vorticity Norm (s^{-1}·mL^{-1})	18,882 (16,767–21,131)	12,909 (10,629–15,526)	10,390 (7695–12,407)	11,338 (9273–14,205)	14,422 (11,800–19,372)	14,150 (11,164–17,990)
Absolute Helicity ($m·s^{-2}·mL^{-1}$)	3084 (2327–3603)	1997 (1287–2729)	1098 (624–1544)	1207 (950–1749)	1873 (1149–2990)	1464 (1059–2263)

Table 2. *Cont.*

Parameter	Anatomical Segments					
	AoR	pAA	dAA	AoA	pDA	dDA
Absolute Local Normalized Helicity Volume (mL)	19.4 (10.5–27.3)	24.8 (18.9–30.2)	15.2 (10.4–21.7)	9.4 (7.0–13.6)	15.6 (12.2–18.2)	17.7 (13.7–19.6)
Volume (mL)	44.1 (25.2–59.8)	53.2 (36.9–59.7)	41.1 (31.0–53.8)	28.6 (20.0–31.5)	38.4 (29.9–45.2)	31.5 (24.2–38.0)
Centerline Length (mm)	31.0 (24.3–37.1)	40.8 (36.6–44.0)	40.0 (36.7–44.3)	37.3 (34.0–38.7)	65.4 (57.0–69.2)	64.1 (58.0–68.9)
Maximal Diameter (mm)	48.7 (40.0–51.3)	44.7 (40.4–46.6)	41.2 (35.4–44.9)	34.3 (31.5–36.3)	31.3 (28.2–32.6)	27.3 (24.9–29.7)
Curvature Radius (mm)	51.4 (42.9–71.1)	38.5 (36.2–46.6)	50.6 (43.3–61.3)	46.1 (40.8–59.7)	45.5 (37.3–53.7)	138.1 (102.0–164.5)

Data notated as the median (Q1–Q3) and presented over all subject and systolic phases. Abbreviations: AoR—aortic root, pAA—proximal ascending aorta, dAA—distal ascending aorta, AoR—aortic arch, pDA—proximal descending aorta, and dDA—distal descending aorta.

A total of 2400 aorta segments were analyzed for the intra- and interobserver reproducibility analysis, see Figure 3. The result of these analyses over all anatomical segments and systolic phases for the validation and training cohort are presented in Table 3 and Supplementary Materials Table S2, respectively.

Table 3. Intra- and interobserver reproducibility: results of the validation cohort.

Study	Bland–Altman		COV (%)	Spearman RankCorrelation Coefficient	Intraclass Correlation Coefficient	LoA_{diff} (%)
	Mean Diff	LoA				
Flow Displacement (%)						
IA-O	−0.1	2.8	19	0.81	0.94	−9
IE-O1	−0.5	4.8	32	0.70	0.84	15
IE-O2	0.1	4.4	30	0.70	0.85	3
IE-O3	0.6	4.1	27	0.79	0.87	7
Flow Jet Angle (°)						
IA-O	0.3	5.0	16	0.92	0.93	−16
IE-O1	−0.3	8.0	25	0.80	0.83	−4
IE-O2	0.2	7.1	23	0.85	0.86	−9
IE-O3	0.5	8.7	27	0.78	0.80	−4
WSS Magnitude (mPa)						
IA-O	0	43	3	1.00	1.00	−15
IE-O1	−33	232	14	0.90	0.93	−10
IE-O2	17	161	10	0.93	0.97	−25
IE-O3	50	242	15	0.89	0.93	30
Axial WSS (mPa)						
IA-O	−0	47	3	1.00	1.00	−59
IE-O1	−30	240	16	0.92	0.94	−58
IE-O2	19	163	11	0.95	0.97	−51
IE-O3	49	244	17	0.92	0.94	51

Table 3. *Cont.*

Study	Bland–Altman		COV (%)	Spearman RankCorrelation Coefficient	Intraclass Correlation Coefficient	LoA_{diff} (%)
	Mean Diff	LoA				
Circumferential WSS (mPa)						
IA-O	−1	39	8	0.98	0.98	11
IE-O1	0	96	19	0.89	0.87	−18
IE-O2	3	73	15	0.93	0.93	0
IE-O3	3	103	20	0.86	0.87	−23
WSS Angle (°)						
IA-O	0.1	3.3	7	0.99	0.99	−47
IE-O1	0.2	8.9	19	0.89	0.94	−8
IE-O2	−0.7	7.5	16	0.95	0.96	−21
IE-O3	−0.9	8.7	18	0.91	0.95	5
Vorticity Norm (s^{-1}·mL^{-1})						
IA-O	37	860	3	1.00	1.00	−40
IE-O1	180	2001	7	0.97	0.98	−4
IE-O2	93	2485	9	0.96	0.97	−22
IE-O3	−87	2779	10	0.96	0.96	6
Absolute Helicity ($m·s^{-2}·mL^{-1}$)						
IA-O	30	223	6	1.00	1.00	−9
IE-O1	−16	394	10	0.98	0.98	14
IE-O2	17	603	15	0.96	0.96	−14
IE-O3	32	631	16	0.96	0.96	21
Absolute Local Normalized Helicity Volume (mL)						
IA-O	0.0	3.3	10	0.99	0.98	−18
IE-O1	0.2	5.9	18	0.95	0.92	6
IE-O2	0.9	8.4	26	0.88	0.86	−28
IE-O3	0.7	6.3	20	0.92	0.91	−10
Volume (mL)						
IA-O	0.2	6.8	9	0.98	0.98	4
IE-O1	1.0	12.7	18	0.93	0.90	−21
IE-O2	1.9	15.7	22	0.89	0.86	−13
IE-O3	0.9	10.8	15	0.94	0.92	−41
Centerline Length (mm)						
IA-O	0.9	7.1	8	0.94	0.97	−7
IE-O1	0.2	11.9	14	0.90	0.92	−36
IE-O2	3.5	12.2	14	0.89	0.92	−20
IE-O3	3.3	8.0	9	0.94	0.96	−53
Maximal Diameter (mm)						
IA-O	−0.2	1.9	3	0.99	0.99	−14
IE-O1	−0.0	4.0	6	0.98	0.97	−3
IE-O2	−0.9	5.0	7	0.98	0.96	−42
IE-O3	−0.9	4.3	6	0.98	0.97	−36

Table 3. *Cont.*

Study	Bland–Altman		COV (%)	Spearman RankCorrelation Coefficient	Intraclass Correlation Coefficient	LoA_{diff} (%)
	Mean Diff	LoA				
Curvature Radius (mm)						
IA-O	2.3	37.2	29	0.87	0.92	30
IE-O1	−2.7	46.4	35	0.77	0.90	14
IE-O2	3.6	42.4	34	0.77	0.90	−72
IE-O3	6.3	43.5	34	0.72	0.92	−70

Characteristics are presented per cohort over all subjects, anatomical segments, and systolic phases (n = 300). All probability values <0.01. Abbreviations: Mean Diff—mean difference; LoA—limits of agreement (1.96× standard deviation); COV—coefficient of variation; IA-O—intraobserver analysis by the first observer with 4 years' experience; IE-O1—interobserver analysis by the first and second observer with 4 and 3 years' experience, respectively; IE-O2—interobserver analysis by the first and third observer with 4 and 1 years' experience, respectively; IE-O3—interobserver analysis by the second and third observer with 3 and 1 years' experience, respectively; WSS—wall shear stress; and LoA_{diff} –relative difference in limits of agreement between the training and validation cohort.

Intra- and interobserver analysis of the hemodynamic parameters demonstrated a good reproducibility in the validation cohort for normalized flow displacement and flow jet angle (LoA $\leq$4.8% and $\leq$8.7° respectively, COV = 16–32%, r = 0.70–0.92, ICC = 0.80–0.94), an excellent reproducibility for vorticity norm (LoA $\leq$2779 $s^{-1}\cdot mL^{-1}$, COV = 3–10%, r = 0.96–1.00, ICC = 0.96–1.00), and a very good reproducibility for absolute WSS_{mag}, WSS_{ax}, WSS_{cir}, WSS_{angle}, absolute helicity and volumes with increased absolute LNH (LoA $\leq$242 mPa, $\leq$244 mPa, $\leq$103 mPa, $\leq$8.9°, $\leq$631 $m\cdot s^{-2}\cdot mL^{-1}$ and $\leq$8.4 mL, respectively; COV = 3–26%, r = 0.86–1.00, ICC = 0.86–1.00). See Supplementary Materials Figures S1–S9 for the corresponding Bland–Altman plots. These plots demonstrated no striking dependency of the measured differences relative to the mean for the analyses and hemodynamic parameters.

Intra- and interobserver analysis of the morphologic parameters demonstrated a very good reproducibility in the validation cohort for volume and centerline length (LoA $\leq$15.7 mL and $\leq$12.2 mm, respectively; COV = 8–22%, r = 0.89–0.98, ICC = 0.90–0.98), and an excellent reproducibility for diameter (LoA $\leq$5.0 mm, COV = 3–7%, r = 0.98–0.99, ICC = 0.96–0.99) and a good reproducibility for curvature radius (LoA $\leq$46.4 mm, COV = 21–35%, r = 0.72–0.87, ICC = 0.90–0.92). See Supplementary Materials Figures S10–S13 for the corresponding Bland–Altman plots. These plots demonstrated no dependency of the measured differences relative to the mean for most analyses and morphologic parameters, except for the maximal diameter, which had a slightly increasing difference relative to the mean for the interobserver analyses.

The intra- and interobserver reproducibility results per anatomical segment are presented in Supplementary Materials Tables S3 and S4, respectively. The intra- and interobserver analysis showed for the validation cohort a similar reproducibility for most morphologic and hemodynamic parameters per segment. However, the reproducibility was slightly decreased within the aortic root for several parameters (i.e., flow displacement, WSS_{mag}, WSS_{ax}, absolute helicity, volumes with increased absolute LNH, aortic segment volume, centerline length, and curvature radius). Furthermore, the reproducibility of the maximal diameter was slightly decreased within the proximal part of the aorta (i.e., the aortic root, proximal and distal ascending aorta) compared to the other anatomical segments further distally to the ascending aorta (intraobserver LoA $\leq$2.7 and $\leq$1.8 mm; interobserver LoA $\leq$7.6 and $\leq$3.3 mm, respectively). Moreover, the reproducibility of WSS_{angle} was slightly decreased within the proximal and distal descending aorta.

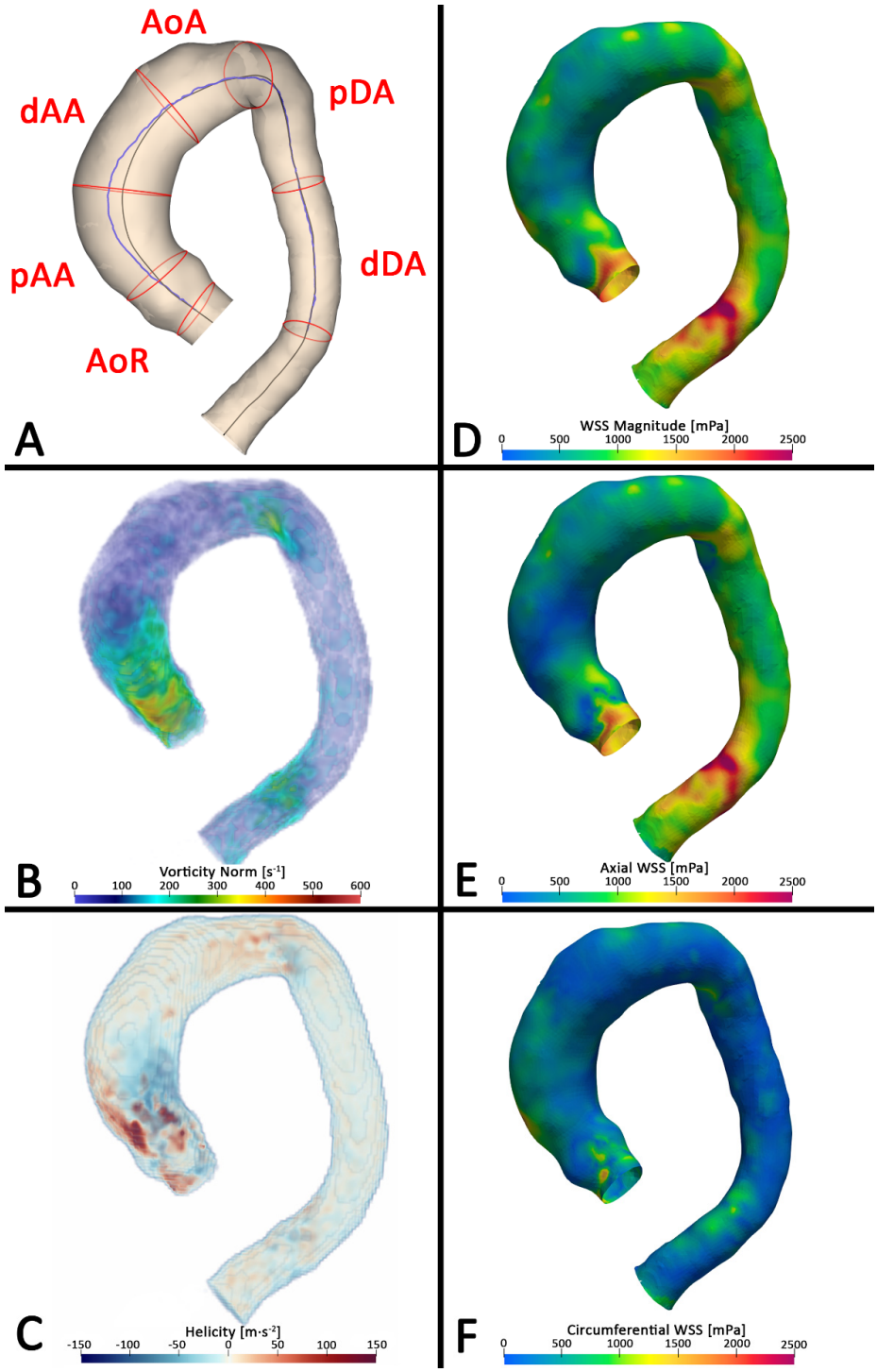

Figure 3. Aortic segments and hemodynamic parameters. Example of a patient (male, 71 years old) with an ascending aorta aneurysm with a diameter of 48 mm. (**A**) Anatomical segments with centerline (black color) and flow displacement line (blue color). (**B**) Vorticity norm. (**C**) Absolute helicity. Positive and negative magnitudes indicate a clockwise and anti-clockwise rotation, respectively. (**D**) Wall shear stress magnitude. (**E**) Axial wall shear stress. (**F**) Circumferential wall shear stress. Abbreviations: AoR—aortic root, pAA—proximal ascending aorta, dAA—distal ascending aorta, AoR—aortic arch, pDA—proximal descending aorta, dDA—distal descending aorta, and WSS—wall shear stress.

Compared to the training cohort, the validation cohort demonstrated reduced LoA over all analyses for morphologic and hemodynamic parameters (LoA_{diff} = −12 [−26–3]%). This improvement was more evident for the morphologic parameters compared to the hemodynamic parameters (LoA_{diff} = −20 [−41–−6]% and −9 [−21–5]%, respectively). Moreover, this improvement was also more evident within the aortic root, proximal and distal ascending aorta compared to the aortic arch, proximal and distal descending aorta (LoA_{diff} = −10 [−35–11] % and 2 [−18–41]%, respectively).

4. Discussion

The main findings of the current study are: (1) hemodynamic parameters (i.e., normalized flow displacement, flow jet angle, WSS_{mag}, WSS_{ax}, WSS_{cir}, WSS_{angle}, vorticity norm, absolute helicity, and volumes with increased absolute LNH) and morphological parameters (volume, centerline length, diameter and curvature radius) can be assessed with very good reproducibility in the thoracic aorta of TAA patients with a TAV, (2) the reproducibility of these parameters is slightly decreased within the aortic root, and (3) the reproducibility is affected by the observer's experience.

The intra- and interobserver analyses generally demonstrated a very good reproducibility for the assessment of hemodynamic parameters in TAA patients with a TAV. Similar results have been described previously for flow displacement, flow jet angle, WSS_{mag}, WSS_{angle}, secondary flow patterns (which are reflected in vorticity and helicity), and volumes with increased absolute LNH in healthy volunteers and in patients with none-to-marginally dilated aortas [11–19,30], but not yet in a clinically relevant patient group, such as patients with TAA. Moreover, the Bland–Altman plots of the current study demonstrated for most hemodynamic parameters and analyses no striking dependency of the measured differences relative to the mean.

Furthermore, the intra- and interobserver analyses demonstrated very good reproducibility of the morphologic parameters in TAA patients with a TAV. Similar reproducibility results have been described previously for volume, centerline length, maximal diameter, and curvature radius in healthy volunteers [25]. However, the current study demonstrated wider LoAs for all morphologic parameters within TAA patients compared to healthy volunteers. These wider LoAs in TAA patients may potentially be associated with the presence of dilation since, for a constant flow rate, the blood velocity is inversely related to the vessel's diameter. Therefore, a larger area of reduced velocity-to-noise ratio is expected for TAA patients compared to healthy volunteers, especially close to the vessel wall. This reduced velocity-to-noise ratio potentially can have a negative influence on the reproducibility of aortic lumen segmentation. However, the velocity-to-noise ratio within these areas may be improved by 4D flow MRI sequences with multiple-velocity-encoding gradients, which consequently may also improve the reproducibility of hemodynamics parameters [31,32].

When analyzing the results per anatomical segment, it was observed that the reproducibility was slightly reduced but still acceptable for most hemodynamic and morphologic parameters within the aortic root. This slight reduction in reproducibility was also seen in the proximal and distal ascending aorta for the maximal diameter. This reduced reproducibility is potentially introduced by the movement of the aortic root and ascending aorta in contrast to the relatively fixed-positioned aortic arch and descending aorta [33–35]. This effect related to the cardiac movement (contraction and relaxation) may further be amplified by the heart rate variation and breathing variation during the acquisition. Alongside, inadequate respiratory compensation or inadequate electrocardiographic gating may also perturbate the 4D flow MRI data. Moreover, within the aortic root, complex secondary flow patterns (recirculating flow) are present [9,36]. Since this recirculating flow has a relatively low velocity compared to the velocity-encoding sensitivity, these recirculating areas have a reduced velocity-to-noise ratio close to the vessel wall and potentially introduce more observer-dependent variability on the aortic lumen segmentation.

The observer-dependent variability of the 3D lumen segmentation was assessed directly by evaluating the variability in morphologic parameters. This analysis also demonstrated, for example, wider LoAs for the maximal diameter within the proximal part of the aorta (i.e., aortic root, proximal and distal ascending aorta) compared to thoracic aorta distal to the ascending part (intraobserver LoA $\leq$2.7 and $\leq$1.8 mm; interobserver LoA $\leq$7.6 and $\leq$3.3 mm, respectively). In contrast, a recent study assessing the interobserver reproducibility of manually measured diameters imaged with computed tomography demonstrated in the aortic root, ascending and descending aorta an LoA of 2.5, 2.1, and 1.9 mm, respectively [37]. For MRI, it is recommended to measure the maximal diameter on an MRI sequence with an isotropic voxel size $\leq$1.5 mm to achieve a clinically acceptable accuracy [38]. Since the 4D flow MRI sequence applied in the current study had an isotropic spatial resolution of 2.5–3.0 mm, the morphologic parameters derived from this sequence should not be used to define the maximal aortic diameter of TAA patients. However, for the quantification of hemodynamic parameters, an isotropic resolution of $\leq$3.0 mm is indicated as sufficient for the 4D flow MRI [23]. Of note, the 4D flow MRI was acquired to assess the patient's aorta hemodynamics and therefore was not meant to describe the patient's aorta morphology (i.e., TAA diameter).

The decreased LoA within the validation cohort compared to the training cohort indicate that the reproducibility likely is affected by the observer's experience, especially for the aortic root, proximal, and distal ascending aorta. Moreover, the observer's experience likely plays a larger role in the assessment of morphologic parameters compared to the hemodynamic parameters, considering the decrease in LoA between the training and validation cohort. This result demonstrates the robustness of the image analysis for the quantification of hemodynamic parameters, despite the observer-dependent variability and experience.

No major limitations were observed for the hemodynamics quantification in the segments of the thoracic aorta. Although no clear reproducibility limitations were observed for TAA patients with a TAV, still some variation is present in the hemodynamic parameters. This variation must be taken into account when these hemodynamic parameters are used for the prediction of progressive dilation and adverse aortic events in TAA patients with a TAV.

A limitation of the present study was the small population size. However, the robustness of the study was improved by including multiple observers, analyzing five systolic phases, and dividing the thoracic aorta into six anatomical segments. This resulted in a total of 2400 lumen segments for which the hemodynamic and morphologic parameters were quantified. Moreover, future research should include patients with other aortic pathologies. Finally, for patients with TAA, no data were available on repeated 4D flow MRI acquisition; thus, interexamination reproducibility could not be assessed.

5. Conclusions

The current study demonstrated a very good reproducibility for all hemodynamic parameters within the thoracic aorta in TAA patients. This allows precise quantification of the patient's aorta hemodynamics from a 4D flow MRI.

Supplementary Materials: The following supporting information can be downloaded at: https://www.mdpi.com/article/10.3390/app12083912/s1, Figure S1: Bland–Altman plots for the normalized flow displacement; Figure S2: Bland–Altman plots for the flow jet angle; Figure S3: Bland–Altman plots for the wall shear stress magnitude; Figure S4: Bland–Altman plots for the axial wall shear stress; Figure S5: Bland–Altman plots for the circumferential wall shear stress; Figure S6: Bland–Altman plots for the wall shear stress angle; Figure S7: Bland–Altman plots for the vorticity norm; Figure S8: Bland–Altman plots for the absolute helicity; Figure S9: Bland–Altman plots for the absolute local normalized helicity volume; Figure S10: Bland–Altman plots for the volume; Figure S11: Bland–Altman plots for the centerline length; Figure S12: Bland–Altman plots for the maximal diameter; Figure S13: Bland–Altman plots for the curvature radius; Table S1: Characteristics of the 4D flow MRI Sequence; Table S2: Intra- and interobserver reproducibility: results of the training cohort; Table S3: Intraobserver reproducibility: results of both cohorts per anatomical segment; Table S4: Interobserver reproducibility: results of both cohorts per anatomical segment; Video S1: Pathline visualization of the 4D flow MRI of a patient with an aortic root aneurysm with a diameter of 52 mm.

Author Contributions: All authors were actively involved in reviewing and editing the manuscript. J.F.J. wrote the original draft version of the manuscript; J.F.J., B.J.C.t.K., R.L.F.v.d.P., P.v.d.B., I.A.D., A.J.H.A.S., H.J.L. and J.J.M.W. contributed to the data curation; J.F.J. and H.C.v.A. developed the in-house developed software; J.F.J., M.J.F.G.R. and B.J.C.t.K. performed the image analysis under supervision of J.J.M.W.; H.J.L., J.J.M.W., A.J.H.A.S., S.S., J.E.W. and B.P.A. contributed to the project administration and funding acquisition. All authors have read and agreed to the published version of the manuscript.

Funding: This work was funded by the Dutch Heart Foundation (CVON2017-08-RADAR).

Institutional Review Board Statement: The study was conducted in accordance with the Declaration of Helsinki and approved by the Institutional Ethics Committee of Leiden University Medical Center (project code G20.149, 9 October 2020).

Informed Consent Statement: Patient consent was waived due to the retrospective inclusion of anonymized clinical data. Patients were not subjected to any research procedures and had the option to withdraw their participation.

Data Availability Statement: Data can be made available upon reasonable request.

Conflicts of Interest: The authors declare no conflict of interest.

References

1. Davies, R.; Gallo, A.; Coady, M.A.; Tellides, G.; Botta, D.M.; Burke, B.; Coe, M.P.; Kopf, G.S.; Elefteriades, J.A. Novel Measurement of Relative Aortic Size Predicts Rupture of Thoracic Aortic Aneurysms. *Ann. Thorac. Surg.* **2006**, *81*, 169–177. [CrossRef] [PubMed]
2. Hiratzka, L.F.; Bakris, G.L.; Beckman, J.; Bersin, R.M.; Carr, V.F.; Casey, D.; Eagle, K.A.; Hermann, L.K.; Isselbacher, E.M.; Kazerooni, E.A.; et al. 2010 ACCF/AHA/AATS/ACR/ASA/SCA/SCAI/SIR/STS/SVM Guidelines for the Diagnosis and Management of Patients with Thoracic Aortic Disease. *J. Am. Coll. Cardiol.* **2010**, *55*, e27–e129. [CrossRef] [PubMed]
3. Members, T.F.; Erbel, R.; Aboyans, V.; Boileau, C.; Bossone, E.; di Bartolomeo, R.; Eggebrecht, H.; Evangelista, A.; Falk, V.; Frank, H.; et al. 2014 ESC Guidelines on the Diagnosis and Treatment of Aortic Diseases. *Eur. Hear. J.* **2014**, *35*, 2873–2926. [CrossRef]
4. Pape, L.A.; Tsai, T.T.; Isselbacher, E.M.; Oh, J.K.; O'Gara, P.T.; Evangelista, A.; Fattori, R.; Meinhardt, G.; Trimarchi, S.; Bossone, E.; et al. Aortic Diameter $\geq$ 5.5 Cm Is Not a Good Predictor of Type A Aortic Dissection. *Circulation* **2007**, *116*, 1120–1127. [CrossRef]
5. Heuts, S.; Adriaans, B.P.; Rylski, B.; Mihl, C.; Bekkers, S.C.A.M.; Olsthoorn, J.R.; Natour, E.; Bouman, H.; Berezowski, M.; Kosiorowska, K.; et al. Evaluating the Diagnostic Accuracy of Maximal Aortic Diameter, Length and Volume for Prediction of Aortic Dissection. *Heart* **2020**, *106*, 892–897. [CrossRef]
6. Glower, D.D. Indications for Ascending Aortic Replacement: Size Alone Is Not Enough. *J. Am. Coll. Cardiol.* **2011**, *58*, 585–586. [CrossRef]
7. Van Hout, M.; Juffermans, J.; Lamb, H.; Kröner, E.; Boogaard, P.V.D.; Schalij, M.; Dekkers, I.; Scholte, A.; Westenberg, J. Ascending Aorta Curvature and Flow Displacement Are Associated with Accelerated Aortic Growth at Long-Term Follow-Up: A MRI Study in Marfan and Thoracic Aortic Aneurysm Patients. *IJC Hear. Vasc.* **2021**, *38*, 100926. [CrossRef]
8. Korpela, T.; Kauhanen, S.P.; Kariniemi, E.; Saari, P.; Liimatainen, T.; Jaakkola, P.; Vanninen, R.; Hedman, M. Flow Displacement and Decreased Wall Shear Stress Might Be Associated with the Growth Rate of an Ascending Aortic Dilatation. *Eur. J. Cardio-Thoracic Surg.* **2021**, *61*, 395–402. [CrossRef]

9. Ramaekers, M.J.; Adriaans, B.P.; Juffermans, J.F.; van Assen, H.C.; Bekkers, S.C.; Scholte, A.J.; Kenjeres, S.; Lamb, H.J.; Wildberger, J.E.; Westenberg, J.J.; et al. Characterization of Ascending Aortic Flow in Patients with Degenerative Aneurysms. *Investig. Radiol.* **2021**, *56*, 494–500. [CrossRef]
10. Bm, S.P.K.; Hedman, M.; Kariniemi, E.; Jaakkola, P.; Vanninen, R.; Saari, P.; Liimatainen, T. Aortic Dilatation Associates with Flow Displacement and Increased Circumferential Wall Shear Stress in Patients Without Aortic Stenosis: A Prospective Clinical Study. *J. Magn. Reson. Imaging* **2019**, *50*, 136–145. [CrossRef]
11. Dux-Santoy, L.; Guala, A.; Teixidó-Turà, G.; Ruiz-Muñoz, A.; Maldonado, G.; Villalva, N.; Galian, L.; Valente, F.; Gutiérrez, L.; González-Alujas, T.; et al. Increased Rotational Flow in the Proximal Aortic Arch Is Associated With Its Dilation in Bicuspid Aortic Valve Disease. *Eur. Heart J. Cardiovasc. Imaging* **2019**, *20*, 1407–1417. [CrossRef] [PubMed]
12. Bissell, M.M.; Hess, A.T.; Biasiolli, L.; Glaze, S.J.; Loudon, M.; Pitcher, A.; Davis, A.; Prendergast, B.; Markl, M.; Barker, A.J.; et al. Aortic Dilation in Bicuspid Aortic Valve Disease. *Circ. Cardiovasc. Imaging* **2013**, *6*, 499–507. [CrossRef] [PubMed]
13. Garcia, J.; Barker, A.J.; Collins, J.D.; Carr, J.C.; Markl, M. Volumetric Quantification of Absolute Local Normalized Helicity in Patients with Bicuspid Aortic Valve and Aortic Dilatation. *Magn. Reson. Med.* **2017**, *78*, 689–701. [CrossRef] [PubMed]
14. Lorenz, R.; Bock, J.; Barker, A.J.; von Knobelsdorff-Brenkenhoff, F.; Wallis, W.; Korvink, J.G.; Bissell, M.M.; Schulz-Menger, J.; Markl, M. 4D Flow Magnetic Resonance Imaging in Bicuspid Aortic Valve Disease Demonstrates Altered Distribution of Aortic Blood Flow Helicity. *Magn. Reson. Med.* **2013**, *71*, 1542–1553. [CrossRef]
15. Sigovan, M.; Hope, M.D.; Dyverfeldt, P.; Saloner, D. Comparison of Four-Dimensional Flow Parameters for Quantification of Flow Eccentricity in the Ascending Aorta. *J. Magn. Reson. Imaging* **2011**, *34*, 1226–1230. [CrossRef]
16. Hope, M.D.; Sigovan, M.; Wrenn, S.J.; Saloner, D.; Dyverfeldt, P. MRI Hemodynamic Markers of Progressive Bicuspid Aortic Valve-Related Aortic Disease. *J. Magn. Reson. Imaging* **2014**, *40*, 140–145. [CrossRef]
17. Reijer, P.M.D.; Sallee, D.; Van Der Velden, P.; Zaaijer, E.R.; Parks, W.J.; Ramamurthy, S.; Robbie, T.Q.; Donati, G.; Lamphier, C.; Beekman, R.P.; et al. Hemodynamic Predictors of Aortic Dilatation in Bicuspid Aortic Valve by Velocity-Encoded Cardiovascular Magnetic Resonance. *J. Cardiovasc. Magn. Reson.* **2010**, *12*, 4. [CrossRef]
18. Geiger, J.; Hirtler, D.; Gottfried, K.; Rahman, O.; Bollache, E.; Barker, A.J.; Markl, M.; Stiller, B. Longitudinal Evaluation of Aortic Hemodynamics in Marfan Syndrome: New Insights from a 4D Flow Cardiovascular Magnetic Resonance Multi-Year Follow-Up Study. *J. Cardiovasc. Magn. Reson.* **2017**, *19*, 33. [CrossRef]
19. Minderhoud, S.C.S.; Roos-Hesselink, J.W.; Chelu, R.G.; Bons, L.R.; Hoven, A.T.V.D.; Korteland, S.-A.; Bosch, A.E.V.D.; Budde, R.P.J.; Wentzel, J.J.; Hirsch, A. Wall Shear Stress Angle Is Associated with Aortic Growth in Bicuspid Aortic Valve Patients. *Eur. Heart J. Cardiovasc. Imaging* **2022**, *22*, jeab290. [CrossRef]
20. Van Der Palen, R.L.F.; Roest, A.A.W.; Boogaard, P.J.V.D.; De Roos, A.; Blom, N.A.; Westenberg, J.J.M. Scan–Rescan Reproducibility of Segmental Aortic Wall Shear Stress As Assessed by Phase-Specific Segmentation With 4D Flow MRI in Healthy Volunteers. *Magn. Reson. Mater. Physics Biol. Med.* **2018**, *31*, 653–663. [CrossRef]
21. Markl, M.; Wallis, W.; Harloff, A. Reproducibility of Flow and Wall Shear Stress Analysis Using Flow-Sensitive Four-Dimensional MRI. *J. Magn. Reson. Imaging* **2011**, *33*, 988–994. [CrossRef] [PubMed]
22. Van Ooij, P.; Powell, A.L.; Potters, W.V.; Carr, J.C.; Markl, M.; Barker, J.A. Reproducibility and interobserver variability of systolic blood flow velocity and 3D wall shear stress derived from 4D flow MRI in the healthy aorta. *J. Magn. Reson. Imaging* **2016**, *43*, 236–248. [CrossRef] [PubMed]
23. Dyverfeldt, P.; Bissell, M.; Barker, A.J.; Bolger, A.F.; Carlhäll, C.-J.; Ebbers, T.; Francios, C.J.; Frydrychowicz, A.; Geiger, J.; Giese, D.; et al. 4D Flow Cardiovascular Magnetic Resonance Consensus Statement. *J. Cardiovasc. Magn. Reson.* **2015**, *17*, 72. [CrossRef]
24. Ms, S.P.; Dyverfeldt, P.; Ebbers, T. Assessment of the Accuracy of MRI Wall Shear Stress Estimation Using Numerical Simulations. *J. Magn. Reson. Imaging* **2012**, *36*, 128–138. [CrossRef]
25. Juffermans, J.F.; Westenberg, J.J.; Boogaard, P.J.; Roest, A.A.; van Assen, H.C.; van der Palen, R.L.; Lamb, H.J. Reproducibility of Aorta Segmentation on 4D Flow MRI in Healthy Volunteers. *J. Magn. Reson. Imaging* **2021**, *53*, 1268–1279. [CrossRef] [PubMed]
26. Wentland, A.L. Editorial for "Reproducibility of Aorta Segmentation on 4D Flow MRI in Healthy Volunteers. *J. Magn. Reson. Imaging* **2021**, *53*, 1280–1281. [CrossRef]
27. Della Corte, A.; Bancone, C.; Dialetto, G.; Covino, F.E.; Manduca, S.; Montibello, M.V.; De Feo, M.; Buonocore, M.; Nappi, G. The Ascending Aorta with Bicuspid Aortic Valve: A Phenotypic Classification with Potential Prognostic Significance. *Eur. J. Cardio Thorac. Surg.* **2014**, *46*, 240–247. [CrossRef]
28. Virtanen, P.; Gommers, R.; Oliphant, T.E.; Haberland, M.; Reddy, T.; Cournapeau, D.; Burovski, E.; Peterson, P.; Weckesser, W.; Bright, J.; et al. SciPy 1.0: Fundamental Algorithms for Scientific Computing in Python. *Nat. Methods* **2020**, *17*, 261–272. [CrossRef]
29. Bland, J.M.; Altman, D.G. Statistical Methods for Assessing Agreement Between Two Methods of Clinical Measurement. *Lancet* **1986**, *1*, 307–310. [CrossRef]
30. Meierhofer, C.; Schneider, E.P.; Lyko, C.; Hutter, A.; Martinoff, S.; Markl, M.; Hager, A.; Hess, J.; Stern, H.; Fratz, S. Wall Shear Stress and Flow Patterns in the Ascending Aorta in Patients with Bicuspid Aortic Valves Differ Significantly from Tricuspid Aortic Valves: A Prospective Study. *Eur. Heart J. Cardiovasc. Imaging* **2012**, *14*, 797–804. [CrossRef]
31. Schnell, S.; Rose, M.J.; Wu, C.; García, J.; Robinson, J.D.; Markl, M.; Rigsby, C.K. Improved Assessment of Aortic Hemodynamics by K-T Accelerated Dual-Venc 4D Flow MRI in Pediatric Patients. *J. Cardiovasc. Magn. Reson.* **2016**, *18*, O96. [CrossRef]

32. Ma, L.E.; Markl, M.; Chow, K.; Vali, A.; Wu, C.; Schnell, S. Efficient triple-VENC phase-Contrast MRI for Improved Velocity Dynamic Range. *Magn. Reson. Med.* **2020**, *83*, 505–520. [CrossRef] [PubMed]
33. Bons, L.R.; Duijnhouwer, A.L.; Boccalini, S.; Hoven, A.T.V.D.; van der Vlugt, M.J.; Chelu, R.G.; McGhie, J.S.; Kardys, I.; Bosch, A.E.V.D.; Siebelink, H.-M.J.; et al. Intermodality Variation of Aortic Dimensions: How, Where and When to Measure the Ascending Aorta. *Int. J. Cardiol.* **2019**, *276*, 230–235. [CrossRef] [PubMed]
34. Bell, V.; Mitchell, W.A.; Sigurðsson, S.; Westenberg, J.J.M.; Gotal, J.D.; Torjesen, A.A.; Aspelund, T.; Launer, L.J.; de Roos, A.; Gudnason, V.; et al. Longitudinal and Circumferential Strain of the Proximal Aorta. *J. Am. Heart Assoc.* **2014**, *3*, e001536. [CrossRef] [PubMed]
35. Rengier, F.; Weber, T.F.; Henninger, V.; Böckler, D.; Schumacher, H.; Kauczor, H.-U.; von Tengg-Kobligk, H. Heartbeat-Related Distension and Displacement of the Thoracic Aorta in Healthy Volunteers. *Eur. J. Radiol.* **2012**, *81*, 158–164. [CrossRef] [PubMed]
36. Kilner, P.J.; Yang, G.Z.; Mohiaddin, R.H.; Firmin, D.N.; Longmore, D.B. Helical and Retrograde Secondary Flow Patterns in the Aortic Arch Studied by Three-Directional Magnetic Resonance Velocity Mapping. *Circulation* **1993**, *88*, 2235–2247. [CrossRef]
37. Dux-Santoy, L.; Rodríguez-Palomares, J.F.; Teixidó-Turà, G.; Ruiz-Muñoz, A.; Casas, G.; Valente, F.; Servato, M.L.; Galian-Gay, L.; Gutiérrez, L.; González-Alujas, T.; et al. Registration-Based Semi-Automatic Assessment of Aortic Diameter Growth Rate from Contrast-Enhanced Computed Tomography Outperforms Manual Quantification. *Eur. Radiol.* **2021**, *32*, 1997–2009. [CrossRef]
38. Van Hout, M.J.; Scholte, A.J.; Juffermans, J.F.; Westenberg, J.J.; Zhong, L.; Zhou, X.; Schalla, S.M.; Hope, M.D.; Bremerich, J.; Kramer, C.M.; et al. How to Measure the Aorta Using MRI: A Practical Guide. *J. Magn. Reson. Imaging* **2020**, *52*, 971–977. [CrossRef]